Onri Jay Benally

12/13/2022

Tunability of Thin Film Tantalum Nitride Grown by Sputtering

University of Minnesota-Twin Cities

Department of Electrical & Computer Engineering

Physical Principles of Thin Film Technology

Table of Contents

I. Background & Motivation

Metal nitride properties can be tuned during vacuum deposition, depending on its intended use in a thin film device. Desired outcomes may include being able to withstand a range of temperatures, oxidation levels, diffusion, mechanical abrasions, and chemical reactivity. The aim could also be towards achieving a certain crystallinity, stability, or electrical conductivity. Each of these characteristics contribute to the longevity and application performance of the film. Here, we present a short review focusing on tantalum nitride (TaN), which can simultaneously achieve many of the desired properties mentioned above, based on how it is grown. By simply varying the growth temperature and mixture of nitrogen (N_2) content or concentration amount with tantalum (Ta) in a growth chamber, various phases of TaN can be realized.

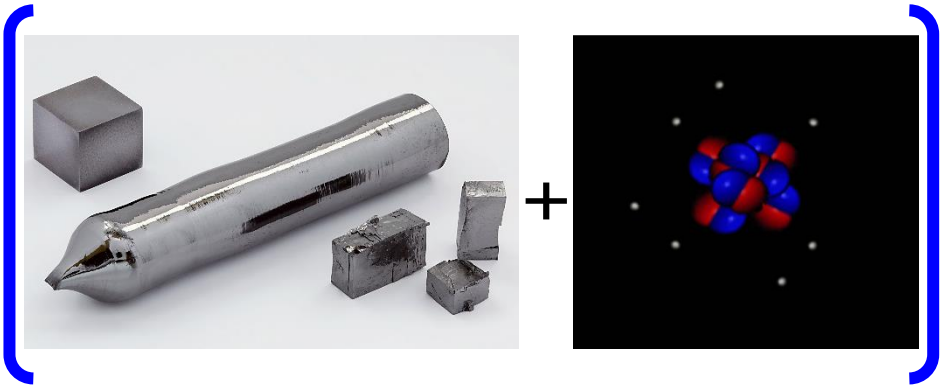

Figure 1 Bare sample of pure Ta and a 3D representation of N. [Taken from Wikimedia Commons].

Like its elemental component Ta, TaN has a high melting temperature, around 3,090^{o}C [18]. This means that it can withstand high heat conditions very well. TaN has numerous manufacturing applications including thin film resistors, protective surface coatings, structural elements in thin film devices, electrical insulators, diffusion barriers, adhesion layers, & spin-orbit torque generation devices for computer memory [1-19, 33]. Generally, as we will see in the following review, TaN with low N_2 concentration is

considered metallic and is electrically conductive, but if the N_2 concentration is relatively high, it exhibits electrical insulator properties [7, 8]. If placed under cryogenic conditions, TaN is shown to exhibit a transition from an electrical insulator to a superconductor [4, 24, 26, 32]. Although there are various deposition methods that can be used to grow TaN, most of the studies highlighted here are grown by magnetron sputtering, due to its low cost and scalability.

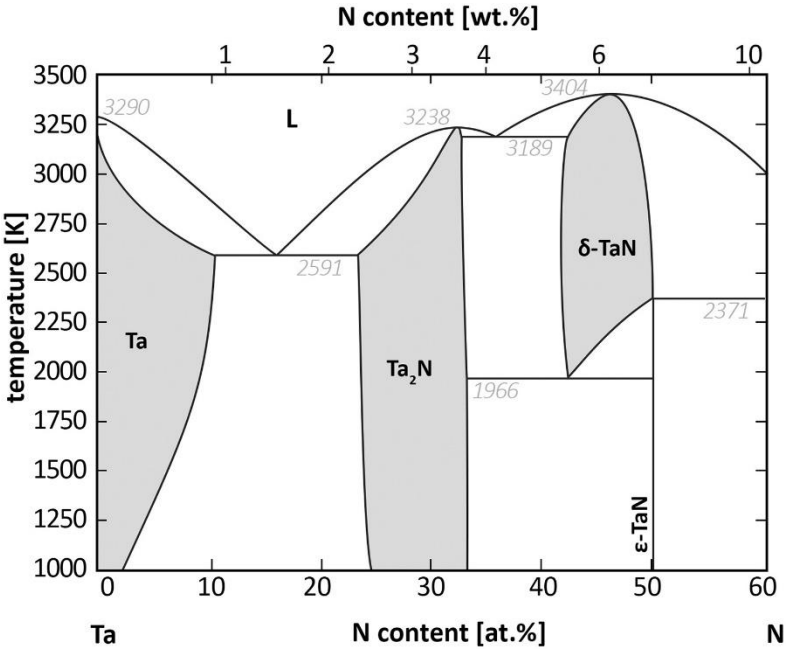

Figure 2 Phase diagram for TaN at various nitrogen concentrations [18].

It can be said that resolution improvements in patterning technology, generally, has led to the ever-increasing density of electronic components and connection lines. In complex multilayered thin film electronic devices, the focus of backend processes for fabrication is on maintaining the high thermal stability and reliability of the deposited metal lines and dielectric isolation [7, 27]. By paying attention to the isolation part, a primary usage of TaN in this common scheme is to prevent oxide diffusion between interfaces (diffusion barrier). This property is characterized by the inherent chemical

inertness of Ta and TaN, especially at high temperatures [8, 27]. In principle, adding more N_2 to the film during growth does not change its chemical stability.

By examining the rich phase diagram of TaN in (Figure 2), notice that various phases of the material can be achieved with percentage control of N_2, from left-to-right. Interestingly, certain other phases form when a range of N_2 percentages are combined with a certain range of growth temperatures. For example, if one wanted to achieve delta-phase TaN, the range of N_2 should be kept between 42% and 50% with a growth temperature range of 1966-3404^{o}C. Thus, we can say that phase composition of TaN determines its overall material properties.

Deposition Methods Overview

Technologically, TaN materials are important because they are currently used as device barrier layers, oxidation protection layers, and even gate metals in purposely doped electronics. Thus, a scalable mode of thin film deposition must be selected based on the project needs. For this reason, sputtering deposition has been widely employed for most of the studies in this review. There are 3 versions of the sputtering deposition system that are noted in the study of TaN: facing-target (FT), direct current (DC), and radio frequency (RF) magnetron sputtering. Overall, these methods are flexible enough to allow careful and consistent power, gas flow, and compatibility with vacuum pumps down to the ultra-high vacuum range as mentioned previously [1-36]. (The gas flows for growth chambers are usually managed through programmed, automated valve controls or by manually turning a valve handle on and off at specific times while watching the pressure indicator).

For the FT sputtering setup, a key advantage is that the samples are protected from the plasma exposure during deposition. This is achieved by having the permanent magnets face parallel to each other with the targets in-between, while the sample substrate(s) are positioned below the targets as shown in (Figure 3). By keeping the field somewhat contained, the resulting plasma during sputtering is also contained. Having this kind of system allows the user to grow a more uniform thin film without compromising the film structure by exposing it to a direct or stray plasma. Additionally, this kind of system typically has robotic components similar to a compact disc changer to allow for pre-loading of multiple substrates that is programmed to load in the chamber once a process is complete [32].

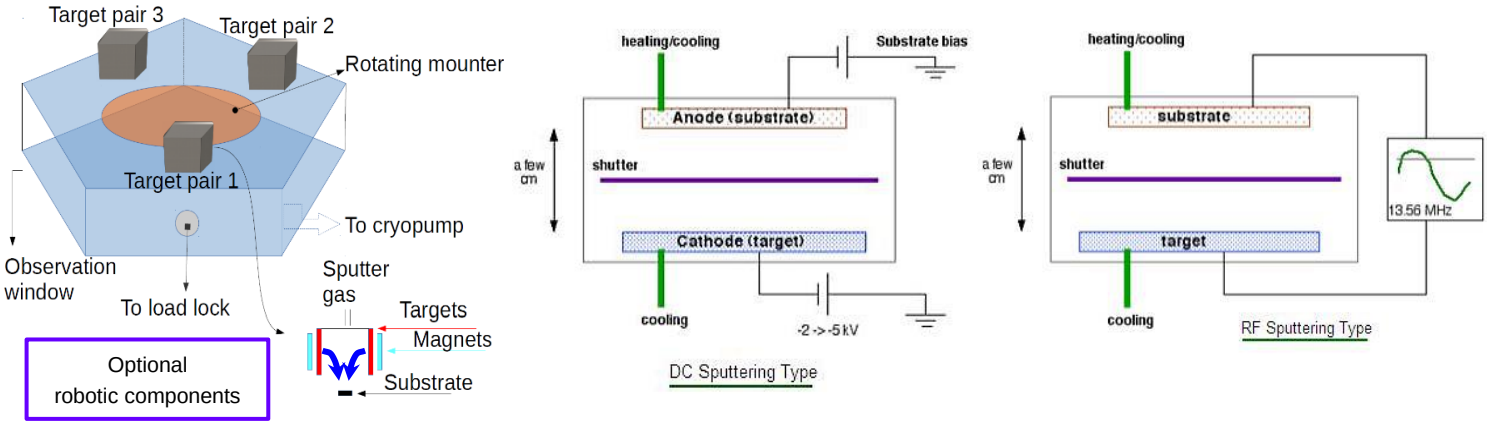

Figure 3 Facing-target magnetron sputtering system (left), direct current magnetron sputtering (center), and radio frequency magnetron sputtering system (right). Taken from: [(Hang, UMN PhD Thesis, 2021) and (aemdeposition.com)].

For the DC sputtering setup, the sample substrates and chamber are typically connected to ground. Although sputtering can be used on both dielectrics (non-conductive) and metals (conductive), electrically conductive targets are the preferred choice for this deposition method because they be applied with a specific substrate bias if needed. By applying a high voltage to the anode and cathode contacts in the chamber, the resulting ionized process gas that is introduced between both contacts will vaporize or

sputter off the target onto the substrate. The underlying permanent ring magnet guides the ionized atoms to an area on the target in the shape of a ring. This relatively simple system allows it to be low-cost, making it a popular choice [1-4, 6, 8-14, 18, 20-21, 24, 26-31, 33, 35-36].

The RF sputtering configuration is similar to the DC sputtering system. The main difference is that the electrically conductive targets are applied with a radio frequency signal, usually fixed at 13.56 MHz due to Federal Communications Commission (FCC) regulations. Here, the voltage being applied to the substrate and target electrical contacts alternate polarity at the frequency mentioned above. As a result, the first cycle of the RF applied signal polarizes the ionized process gas and the target surface, then the second cycle reverses polarity, causing an ejection of the vaporized target atoms toward the substrate surface. Although RF sputtering can be used for both electrically conductive and non-conductive targets, it is most often used for non-conductive dielectric materials at low deposition rates. [7, 25, 34]. In this review of course, we are interested in the use of conductive Ta targets.

II. Design Process Flow (Deposition Parameters)

Since thin film performance can vary by thickness, all of the studies examined here were carried out on layers of TaN as thin as 1.1 nm, with a maximum thickness of 960 nm as seen in (Table 1). To clarify, argon (Ar) was the sputtering process gas used for vaporizing the target in all the studies of this review, while N_2 was used as a mixture, percentage, or ratio added to the deposited Ta to form TaN. Note that

sputtering power has a very wide range, from the nanowatt to kilowatt level, a difference of 4 orders of magnitude. A number of compatible substrate types were also used. All vacuum chamber conditions in these studies are below the 10^{-3} Torr range, with the lowest being around 10^{-11} Torr. It is interesting to note that while reading the texts, both substrate temperature and growth temperature were used alternately from article-to-article. This was confusing. So, upon asking for clarification from the active thin films community/ experts at the University of Minnesota, it was confirmed that growth and substrate temperature are basically the same thing and are used interchangeably.

Film Thicknesses	**Sputtering Power**	**Substrate Types**	**Growth Temperatures**	**Average Total Gas Flow**	**Nitrogen Ratio $N_2/(Ar+N_2)$**
1.1 - 960 nm	10 nW** - 1.2 kW	Fused quartz, Si, MgO, 316L SS*, Glass, Ti, Cr12MoV steel, LiNbO3, Si3N4, Al2O3	20°C - 800°C	30 sccm	0 – 75%

Table 1 List of sputtered growth parameters for TaN.
*SS: Stainless Steel, **Low energy DC sputtering

III. Nitrogen Concentration Effects

Surface Roughness

Concentration of N_2 is provided by a ratio or percentage as noted on the last column to the right in (Table 1). While searching for a comparison of thin film growth conditions, one will notice that the parameters are only mentioned in experimental studies [1-36]. Thus, it is important to find keywords such as *"substrate", "deposition", "roughness", and "interface"*. Interestingly, theory articles that focus on numerical

calculations all were missing these important terms. Subsequently, they tend to be open-ended, without a conclusion section.

Nevertheless, for the studies referenced in this review, N concentration has been shown to affect the surface roughness of the film. The importance of this film characteristic is that it shows a layer adhesion potential at the nanoscale. Generally, when a sample surface is scanned by the probe of an atomic force microscope (AFM), a smooth surface shown by the resulting 3D analysis means that the surface adhesion is stronger. On the other hand, if the resulting AFM scan shows a rough surface topology, then the surface adhesion is weaker. However, different surfaces may vary in roughness and one way to judge the films by the same standard is to purposely etch the surface physically or chemically for a few seconds before performing an AFM scan [33-36]. If interested in the grain size of the films, then the AFM results will allow for grain size measurement based on the lateral change in brightness on the 2D scans as shown in (Figure 4).

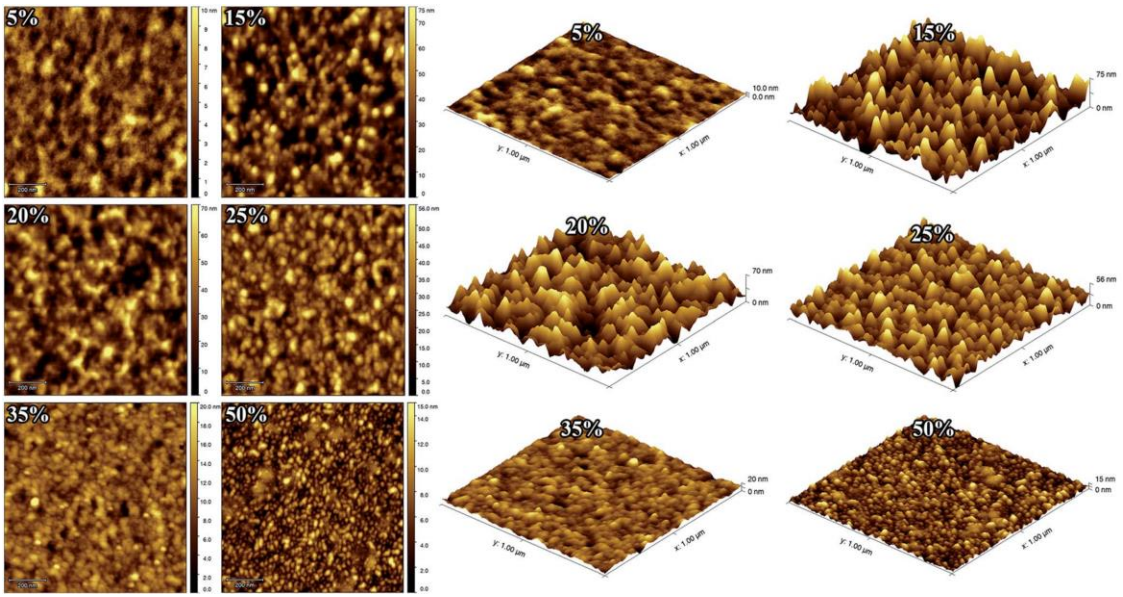

Figure 4 2D and 3D AFM images of TaN deposited at various N_2 flow ratios for a 300 nm thick film [1].

Looking closer at (Figure 4), the surface roughness increases dramatically from an average height of 4.3 nm to 28 nm when increasing the N_2 concentration from 5% to 15%. As the N_2 concentration increases from 35% to 50% however, the surface roughness drops back down to an average height of 6.1 nm. This shows that in the intermediate range of N_2 (15-25%) concentrations, the sample adhesion is low, but in the extremes (5%, 50%), the sample adhesion is high due to a smoother surface. All other studies are in agreement with the surface roughness data for a fixed film thickness, as indicated in (Figure 5). Despite the N_2 content plot only maxing out at 15%, it still shows a similar increase in roughness that was indicated in (Figure 4). Although the samples grown by (Alishahi et al.) are about a third of the thickness of the samples grown by (Riekkinen et al.), the roughness results are consistent. This should be expected as the fixed film or minimum variation in film thickness seems to follow this rule.

$[N_2]$ (%)	2	5	15	20	25	35	50
Mean height (nm)	1.1	4.3	28	30.4	26.5	10.2	6.1
R_a (nm)	0.4	1.4	11.8	11.6	8.4	1.9	2.1
R_{rms} (nm)	0.5	1.7	14.7	14.1	10.9	2.4	2.6
ζ (nm)	63	53	40	42	30	28	22

Table 2 Surface parameters from the AFM scan in Figure 4 [1].

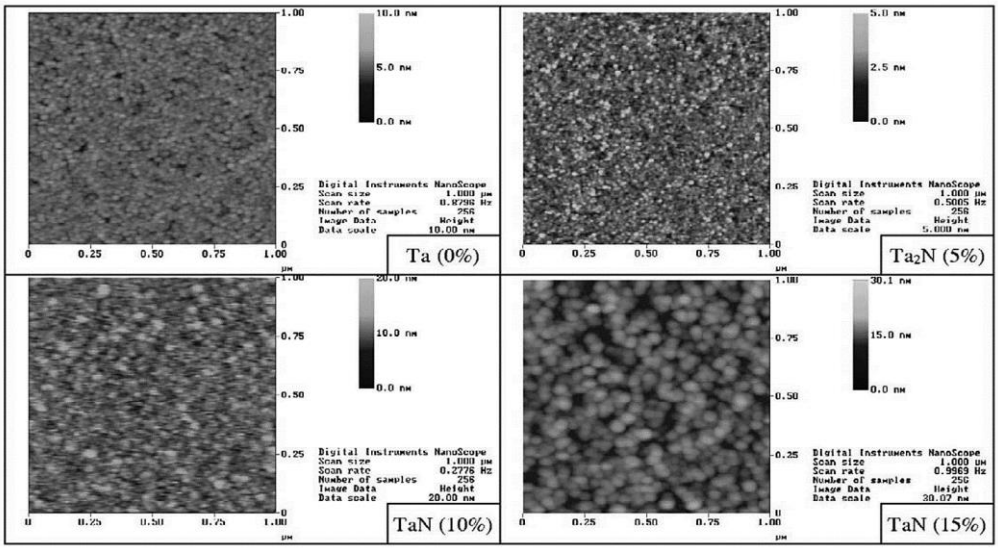

Figure 5 2D AFM images of deposited TaN with an average thickness of 103 nm at various N_2 concentrations [28].

On the other hand, if one were to keep the N_2 concentration at a fixed value, such as 5% or less, then it is possible to notice an increase in surface roughness by growing the TaN film thicker. This is shown in (Figure 6) with supporting RMS roughness data shown in (Figure 7), prepared by (Cuong et al.). One unique paper from (Lee et al.) shows an experiment on how a 411 nm TaN film was tested on its adhesive strength via a cured resin, attached to a load cell for measurement. Unfortunately, there weren't any other references on nitride films being tested in this way. However, it is convenient to know that chemical adhesion to a cured substance, such as resin, can be

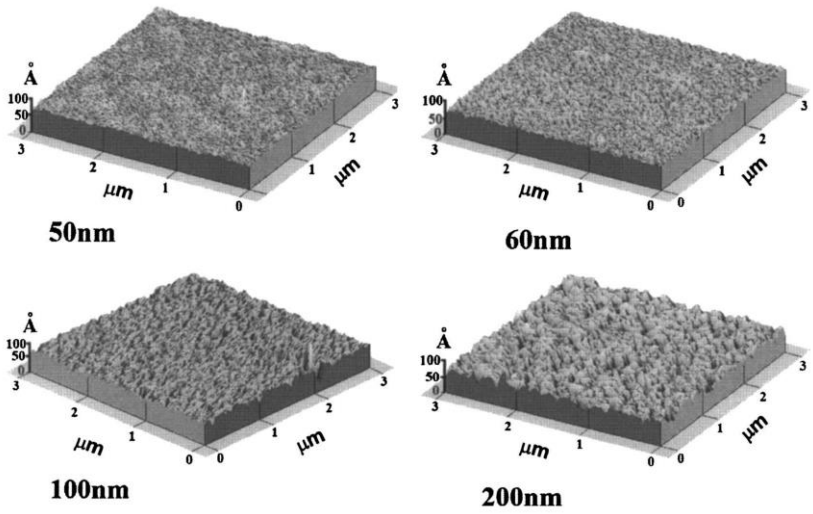

Figure 6 3D AFM scan of Ta_2N films of different thicknesses, deposited at a fixed 3% N_2 flow ratio [9].

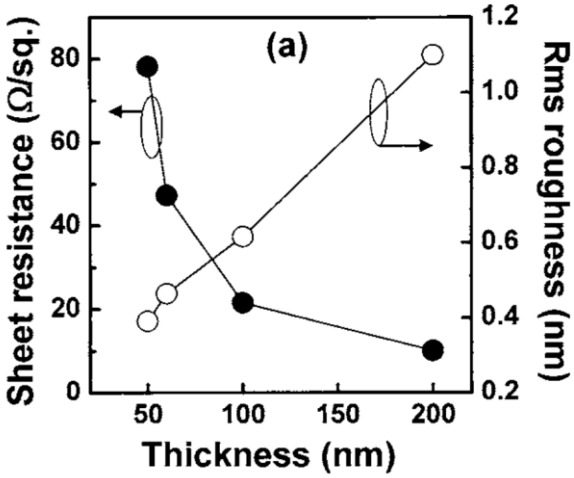

Figure 7 Variation in sheet resistance and RMS roughness as a function of Ta_2N film thickness, deposited at a fixed N_2 ratio of 3% [9].

enhanced greatly, nearly 4 times as much, when the substrate of the TaN film has been heated during growth (Figure 8).

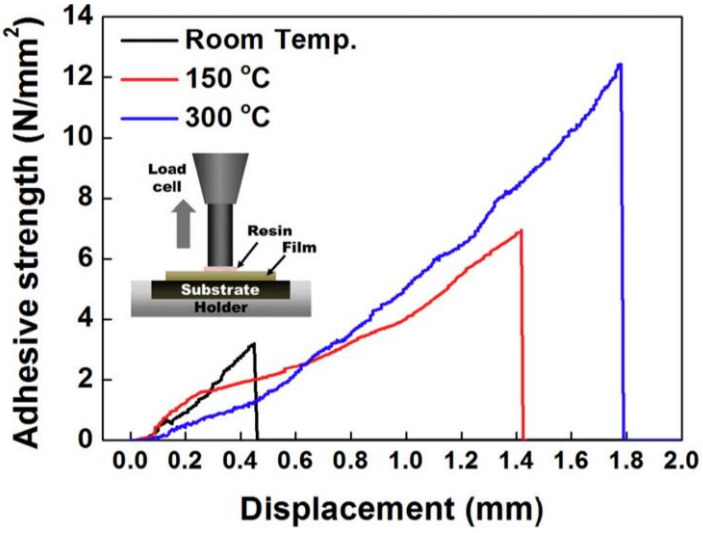

Figure 8 Plot of adhesive strengths on 411 nm deposited TaN films as a function of displacement for various substrate temperatures

Crystal Structure

If interested in the crystal structure of TaN films grown by sputtering, then X-ray diffraction is a widely used technique. A study by (Okuno et al.) shows a plot of how various crystal directions can be achieved by modifying the N_2 concentration during growth. If we look at (Figure 9), notice how TaN (101) peak is dominant with a 5% N_2 concentration, TaN (100) for 10% N_2 concentration, and TaN (200) for 15% N_2

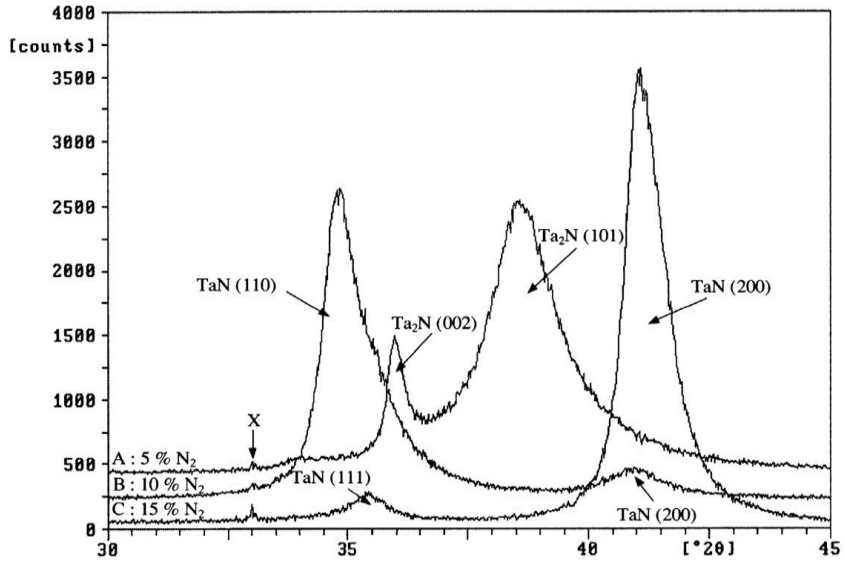

Figure 9 X-Ray Diffraction Plot vs. Various Nitrogen Concentrations [27].

concentration. This is a strong correlation to keep in mind because, clearly, N_2 in slightly higher mixtures for sputtering really changes the crystal direction of the final film. This is further supported by all other studies in the reference section of this review. They all show similar plots of dominant peaks that change by small differences in N_2 mixture [1-32].

Electrical Resistivity

To measure the electrical properties of TaN, point-probe measurement systems are typically employed. It involves a needle contact to the surface of an un-patterned sample that has been deposited with material. In this case, TaN tends to retain its metallic properties at lower N_2 concentrations for N_2 mixtures at or below 20%. This is supported by the resistivity data similar to the ones shown in (Figure 10-11). In previous sections of this review, one can see that a smoother, stable film for layer stacking is obtained by either low N_2 or relatively higher N_2 mixtures (Figure 4-8) found in [1, 9, 20, 28]. This means that if you wanted to use TaN thin films in a stacked nanostructure, including devices, then choosing a smooth surfaced, stable phase of TaN is preferred. However, if you wanted a non-metallic, non-electrically conductive version of TaN to be used in a stacked nanostructure, then a higher N_2 sputtered film should be used. For example, in (Figure 11) notice that the resistivity value stays below 3 mΩ cm up to the 20% N_2 concentration.

In most cases, deposited films are intended for applications in the so-called "normal state" and conditions that are at or slightly above room temperature. As a

result, superconducting perspectives of TaN are not as widely investigated. According to 4 different studies, TaN was measured in low-temperature conditions, using liquid Helium (He), for measuring resistivity [4, 24, 26, 32]. (Figure 12) shows a plot of δ-TaN film with a thickness of 10 nm that was grown with a N_2 concentration of 44%. Here we can see that resistivity is relatively high in normal conditions and this would make sense because other studies show that resistivity of all thin film TaN phases increase dramatically with a continuous upward trend as the N_2 mixture goes beyond 25% (Figure 10 - 11). As mentioned earlier, what makes this fascinating is that when the TaN film is exposed to cryogenic conditions, the resistivity drops to zero at 4K, showing that if one wanted a material to be electrically insulating at room temperature (300k), but switch to a superconductor at a low-temperature (4K), then picking a high N_2 TaN, regardless of phase, can be made.

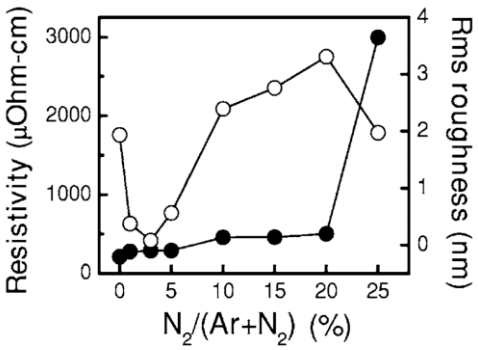

Figure 10 Variation of room temperature resistivity and RMS roughness of deposited TaN as a function of N_2 concentration [8].

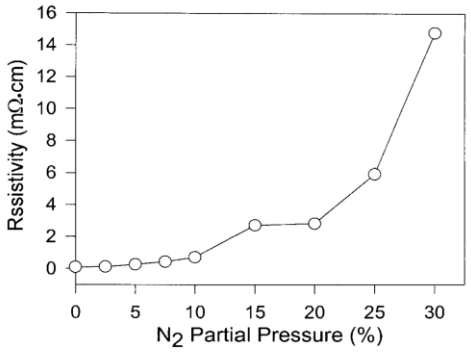

Figure 11 Variation of room temperature resistivity of TaN deposited on glass substrate as a function of N_2 concentration

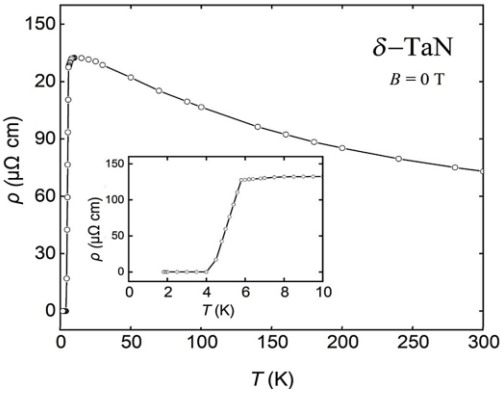

Figure 12 Plot of δ-TaN resistivity as a function of temperature with a fixed N_2 concentration of 44% [32].

Mechanical Hardness

Another important property of TaN that contributes to its endurance is its mechanical hardness. On a macro scale, a well-known testing scheme for material surface resistance to abrasion or mechanical scratches is by the Mohs hardness scale. It usually involves scratching the surface of a material of interest and closely inspecting the depth of the scratch. A common method among the thin films community for testing the mechanical hardness for nanostructures is the nano indentation technique. This is done by penetrating the surface of a film and measuring the resulting depth of the physically deformed features. Although these methods will not be covered in detail here, it is generally known by the thin films community that amorphous structures are resistant to oxidation. If we look at the 2 plots from (Figure 13 and 14), the effect of N_2 content on hardness follows and upward trend and hits a peak in the intermediate range (out of 100%). This is then followed by a reduction of hardness at higher ranges of N_2 mixture. (Figure 13) tries to compare the similarities between TaN films grown by different sputtering deposition methods and here we can see that the curve is pretty close for DC, pulsed DC, and hi-power impulse magnetron sputtering techniques.

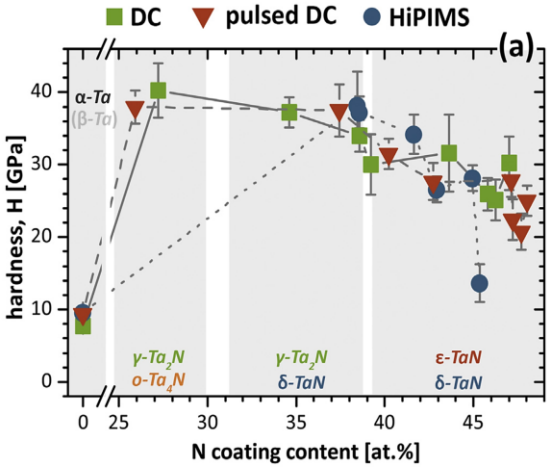

Figure 13 Mechanical hardness (H) of various phases of deposited TaN as a function of their N_2 content [18].

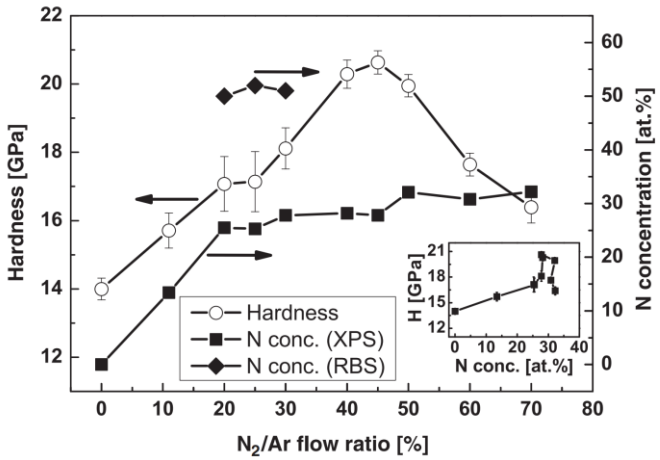

Figure 14 Extensive plot of mechanical hardness as a function of N_2 concentration on deposited TaN [3].

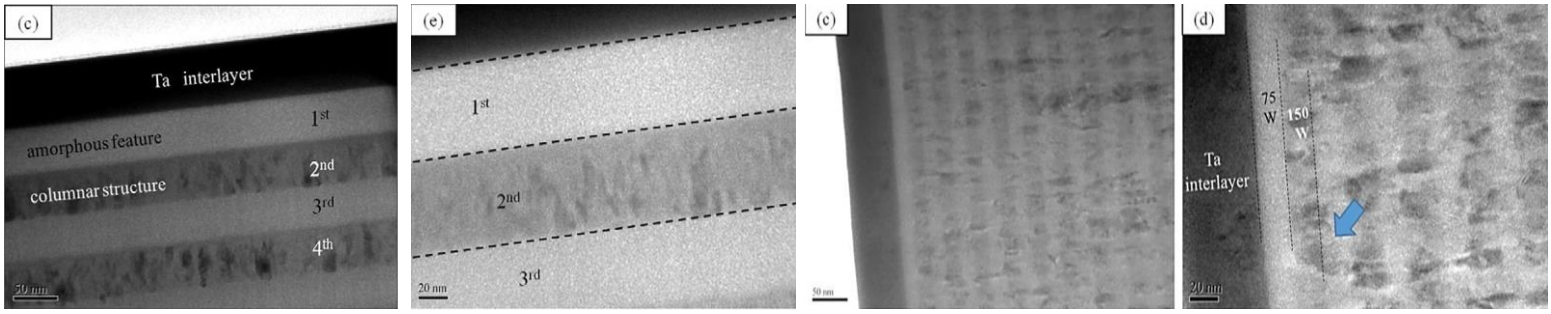

Figure 15 Cross-sectional TEM scan of alternating TaN amorphous-crystalline multilayers (2 on the left) vs. alternating sputter power all-crystalline multilayers of TaN (2 on the right) [36].

If we examine (Figure 15), an experiment was conducted to see if alternating between amorphous and crystalline TaN or alternating between different sputtering powers during growth of crystalline TaN would affect the overall hardness. The results, along with supporting indentation data, showed that the alternating amorphous-crystalline multilayer sample was softer while the other all-crystalline multilayer TaN was harder and thus more resistant to mechanical scratches, indentation, and abrasion. However, this does not necessarily mean that the harder, overall crystalline TaN sample would resist oxidation better than the amorphous integrated one. The clear amorphous layers basically prolong the erosion path due to their smaller grains and this is what gives it its higher corrosion resistance when discussed [36].

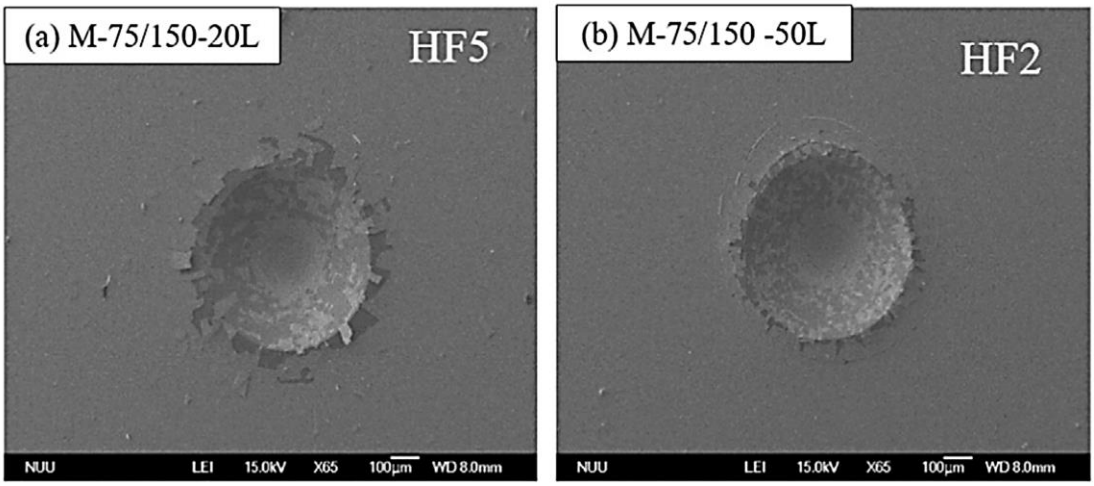

Figure 16 SEM scans of 2 samples of multilayer TaN samples tested with Rockwell hardness indentation points. On the left is the sample with integrated amorphous layers. The right image is from the sample with an overall crystalline structure [36].

V. Device Integration and Interface Compatibility

Knowing that TaN can be prepared with conductive, metallic properties or as an insulator down to the single nanometer level, devices have already been integrated so far for testing. In (Figure 7), there is a semiconductor oxide-based transistor that faced the issue of oxidation of the source/drain electrode, which further led to unwanted oxygen vacancies, which further led to unstable current flow in during device parameter testing (Figure 20). As a result, TaN was selected as a source/drain layer in the transistor and compared between poor N_2 and rich N_2 grown samples. Given that nitrides with low N_2 are not as resistant against oxygen diffusion, it would make sense that oxygen gets in the TaN layer with poor N_2. This is shown very clearly in (Figure 18 and 19). Since TaN tends to have metallic properties with N_2 concentrations at or below 20%, then the rich N_2 samples used in the study by (Okuno et al.) should be around that upper limit. There

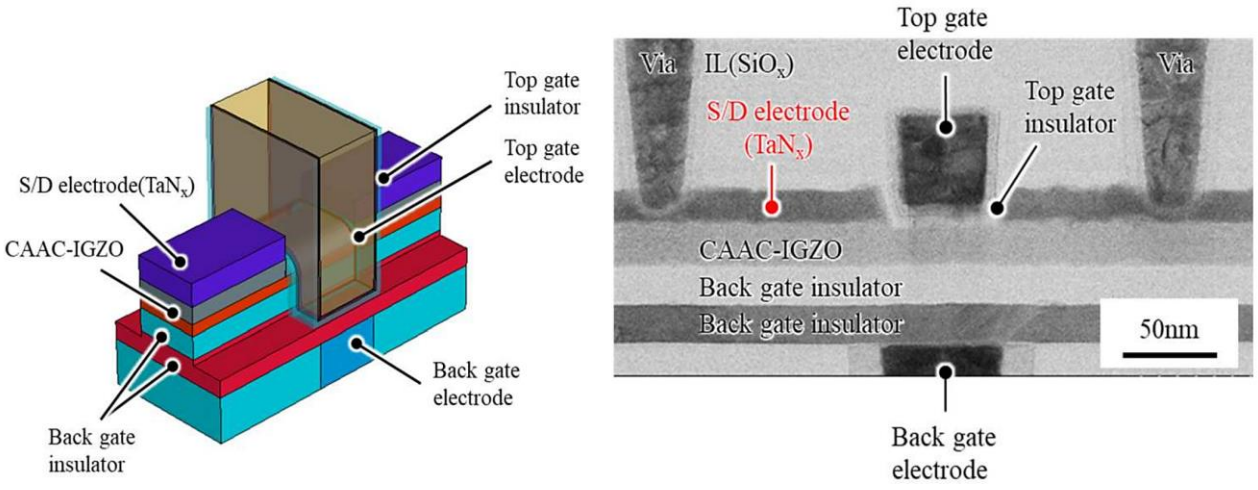

Figure 17 3D schematic bird's eye view of an FET device designed with oxidation resistant TaN layers [27].

are similar studies that follow a similar scenario in [6, 11, 29, 35], depending on whether low thickness electrical insulation or conductivity was needed.

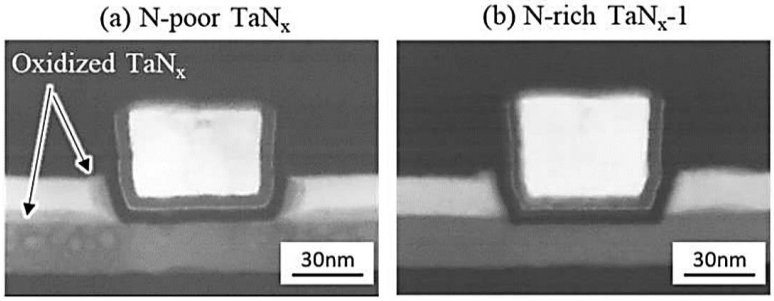

Figure 18 Comparison of low N_2 grown and high N2 grown TaN being used as an electrode, interfaced with an oxide semiconductor layer [27].

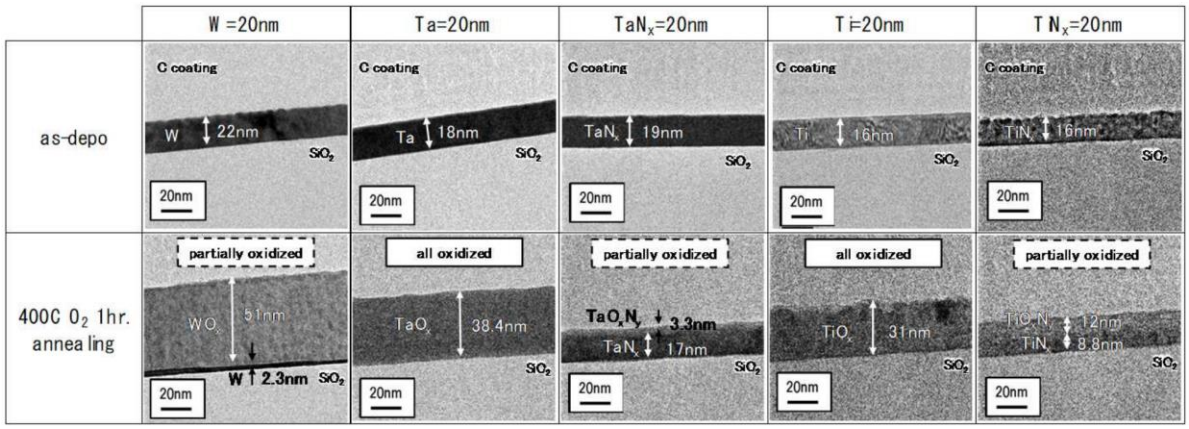

Figure 19 Comparison of oxidation diffusion for various nitride, elemental, and semiconductor oxide layers interfaced with each other before and after oxide thermal annealing [27].

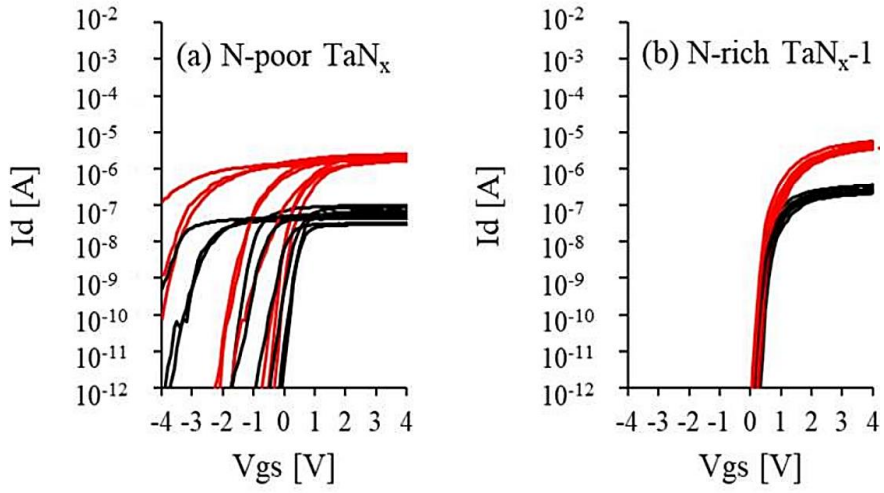

Figure 20 Comparison of current stability plots from the FET source and drain [27].

VI. Summary

TaN has the ability to behave like a metal or an insulator and can adhere better to surfaces based on mixture of N_2 during sputtered growth. A few references contain comparisons of TaN sputtering with other vacuum deposition methods for a better understanding. A phase diagram was provided as a general guide to predict the individually desired material phase information based on how much N_2 and substrate heat was added. Although the phase diagram did not present any direct crystallographic direction predictions, most studies were able to provide N_2 concentration dependent TaN crystal directions by spectroscopy and diffraction analysis. Here, in TaN thin films with sub-micron thickness, various methods of testing were explored from article-to-article to check for consistencies in data presentation. Although some samples were measured under limited conditions, the general trend tended to agree with many other studies. A few were niche, such as the case with low-temperature components that used TaN in extreme conditions.

References

1. Alishahi, M. et al. (2016). Structural properties and corrosion resistance of tantalum nitride coatings produced by reactive DC magnetron sputtering. *RCS Advances*.

2. Baik, S. I. et al. (2020). Microstructural evolution of tantalum nitride thin films synthesized by inductively coupled plasma sputtering. *Applied Microscopy*.

3. Bernoulli, D. et al. (2013). Magnetron sputter deposited tantalum and tantalum nitride thin films: An analysis of phase, hardness and composition. *Thin Solid Films*.

4. Breznay, N. P. et al. (2017). Superconductor to weak-insulator transitions in disordered tantalum nitride films. *Physical Review B*.

5. Chaudhuri, S. et al. (2013). Fabrication of superconducting tantalum nitride thin films using infrared pulsed laser deposition. *Journal of Vacuum Science & Technology A*.

6. Chen, H. R. et al. (2016). Mechanisms of Low-Temperature Nitridation Technology on a TaN Thin Film Resistor for Temperature Sensor Applications. *Nanoscale Research Letters*.

7. Chen, S. F. et al. (2017). Effect of nitrogen flow rate on TaN diffusion barrier layer deposited between a Cu layer and a Si-based substrate. *Ceramics International*.

8. Cuong, N. D. et al. (2006). Characterization of Tantalum Nitride Thin Films Deposited on SiO2⁄Si Substrates Using dc Magnetron Sputtering for Thin Film Resistors. *Journal of The Electrochemical Society.*

9. Cuong, N. D. et al. (2006). Effect of film thickness on the electrical properties of tantalum nitride thin films deposited on SiO2/Si substrates for Π-type attenuator applications. *Journal of Vacuum Science & Technology B.*

10. Firouzabadi, S. S. et al. (2017). Effect of nitrogen flow ratio on nano-mechanical properties of tantalum nitride thin film. *Journal of Alloys & Compounds.*

11. Gerlich, L. et al. (2013). Interface engineering for the TaN/Ta barrier film deposition process to control Ta-crystal growth. *Microelectronic Engineering.*

12. Gholami, M. et al. (2022). Fabrication and Characterization of TaxN Thin Films Deposited by DC Magnetron Sputtering Technique: Application in Microelectronic Devices. *Brazilian Journal of Physics.*

13. Grosser, M. et al. (2017). Microstructure and mechanical properties of sputter deposited tantalum nitride thin films after high temperature loading. *Thin Solid Films.*

14. Hashizume, T. et al. (2011). Fabrication of Tantalum nitride thin film using the low vacuum magnetron sputtering system. *IOP Conf. Series: Materials Science and Engineering.*

15. Hee, A. C. et al. (2019). Characterization of tantalum and tantalum nitride films on Ti6Al4V substrate prepared by filtered cathodic vacuum arc deposition for biomedical applications. *Surface & Coatings Technology.*

16. Katzer, D. S. et al. (2014). Silicon nitride thin films deposited using electron-beam evaporation in an RF plasma MBE system. *Journal of Vacuum Science & Technology B.*

17. Kim, M. et al. (2022). The effective Work-Function of atomic layer deposited TaN thin film using TBTDET precursor and NH3 reactant gas. *Applied Surface Science.*

18. Koller, C. M. (2018). Structure, phase evolution, and mechanical properties of DC, pulsed DC, and high-power impulse magnetron sputtered Ta–N films. *Surface & Coatings Technology.*

19. Lang, A. C. et al. (2021). Phase Identification and Ordered Vacancy Imaging in Epitaxial Metallic Ta2N Thin Films. *ACS Appl. Mater. Interfaces.*

20. Lee, D. W. et al. (2018). Reliability and characteristics of magnetron sputter deposited tantalum nitride for thin film resistors. *Thin Solid Films.*

21. Liu, X. et al. (2011). Effect of deposition and annealing temperature on mechanical properties of TaN film. *Applied Surface Science.*

22. Marchack, N. et al. (2019). Utilizing surface modification in plasma-enhanced cyclic etching of tantalum nitride to surpass lithographic limits. *Plasma Processes & Polymers.*

23. Marchack, N. et al. (2020). Control of surface oxide formation in plasma-enhanced quasiatomic layer etching of tantalum nitride. *Journal of Vacuum Science & Technology A.*

24. Müller, M. et al. (2021). Growth optimization of TaN for superconducting spintronics. *Materials for Quantum Technology.*

25. Nie, H. B. et al. (2001). Structural and electrical properties of tantalum nitride thin films fabricated by using reactive radio-frequency magnetron sputtering. *Applied Physics A.*

26. Nieto, A. et al. (2022). Synthesis of Superconductive TaN Thin Films by Reactive DC Sputtering. *Journal of Electronic Materials.*

27. Okuno, N. et al. (2021). Source/Drain Engineering by Tantalum Nitride (TaNx) Electrode for Boosting OSFET Performance. *IEEE International Electron Devices Meeting (IEDM).*

28. Riekkinen, T. et al. (2002). Reactive sputter deposition and properties of TaN thin films. *Microelectronic Engineering.*

29. Rossnagel, S. M. (2002). Characteristics of ultrathin Ta and TaN films. *Journal of Vacuum Science & Technology B.*

30. Rudolph, M. et al. (2018). Influence of backscattered neutrals on the grain size of magnetron-sputtered TaN thin films. *Thin Solid Films.*

31. Shostachenko, S. A. et al. (2017). Thermal stability of tantalum nitride based thin film resistors. *IOP Conf. Series: Materials Science and Engineering.*

32. Swatek, P. W. et al. (2022). Room temperature spin-orbit torque efficiency in sputtered low-temperature superconductor δ-TaN. *Physical Review Materials.*

33. Thorsteinsson, D. O. et al. (2015). Morphology of Tantalum Nitride Thin Films Grown on Fused Quartz by Reactive High Power Impulse Magnetron Sputtering (HiPIMS). *Materials Research Society.*

34. Tsukimoto, S. et al. (2004). Microstructure of amorphous tantalum nitride thin films. *Thin Solid Films.*

35. Vogel, U. et al. (2017). Interface and stability analysis of Tantalum- and Titanium nitride thin films onto Lithiumniobate. *Applied Surface Science.*

36. Yang, Y. H. et al. (2016). Microstructure evolution and protective properties of TaN multilayer coatings. *Surface & Coatings Technology.*